Heliyon 10 (2024) e36676

Contents lists available at ScienceDirect

Heliyon

journal homepage: www.cell.com/heliyon

Research article

Electrical breakdown in liquid-phase processing on an enhancement of 7-hydroxymitragynine conversion from mitragynine in *Mitragyna speciose* (Kratom)

Weerasak Samee [a], Khanit Matra [b,*], Nattawut Lakkham [b], Beelawan Dongkaew [b], Passakorn Sumkhum [b], Wutthichok Sangwang [c], Wasin Nupangtha [d], Jiraporn Promping [c]

[a] *Department of Pharmaceutical Chemistry, Faculty of Pharmacy, Srinakharinwirot University, Nakhonnayok, 26120, Thailand*
[b] *Department of Electrical Engineering, Faculty of Engineering, Srinakharinwirot University, Nakhonnayok, 26120, Thailand*
[c] *Thailand Institute of Nuclear Technology (Public Organization), Ongkharak, Nakhon Nayok, 26120, Thailand*
[d] *Faculty of Science and Agricultural Technology, Rajamangala University of Technology Lanna, Nan Campus, Nan 55000, Thailand*

A R T I C L E I N F O

Keywords:
Electrical breakdown in liquid-phase (EBL)
Advanced oxidation processes (AOPs)
Mitragynine (MG)
7-Hydroxymitragynine (7-OH MG)
Plasma technology

A B S T R A C T

This study investigates the impact of the Electrical Breakdown in Liquid-phase (EBL) process on alkaloid transformation in *Mitragyna speciose* (Kratom) leaves, focusing on the conversion of mitragynine (MG) to 7-hydroxy mitragynine (7-OH-MG) by using advanced oxidation processes (AOPs). A novel reactor has been developed to enhance plasma exposure to Kratom leaf powdered solutions during the EBL process. Two distinct electrical voltage characteristics, half-positive and negative half-waves, have been utilized for the EBL, with an output voltage of 4.57 kV_{peak} at a no-load condition and a frequency of 50 Hz. The experimental findings demonstrate a time-dependent enhancement in the transformation process. The highest yield of 7-OH-MG, reaching 2,485 ± 134 μg/g of dried Kratom leaves weight, has been attained with the EBL processing generated by positive half-wave voltage after 20 min of EBL exposure. Notably, the EBL processing generated by positive half-wave voltage has outperformed the one generated by negative half-wave voltage by a significant factor of 2.01.

Nomenclatures

Abbreviations	Meaning
7-OH-MG	7-hydroxymitragynine
ANOVA	Analysis of variance
AOPs	Advanced oxidation processes
CCD	Compact charge-coupled device
I_D	Discharge current
V_D	Discharge voltage
pKa	Dissociation constant
EBL	Electrical Breakdown in Liquid-phase
NV-EBL	EBL processing generated by the negative half-wave supplied voltage

(*continued on next page*)

* Corresponding author.
E-mail address: khanit@g.swu.ac.th (K. Matra).

https://doi.org/10.1016/j.heliyon.2024.e36676
Received 6 November 2023; Received in revised form 7 August 2024; Accepted 20 August 2024
Available online 22 August 2024

(*continued*)

PV-EBL	EBL processing generated by the positive half-wave supplied voltage
EC	Electrical conductivity
HWVD	Half-wave voltage doubler
HPLC	High-performance liquid chromatography
LOD	Limit of detection
LOQ	Limit of quantification
MG	Mitragynine
NV	Negative half-wave supplied voltage
OES	Optical emission spectra
PV	Positive half-wave supplied voltage
RNSs	Reactive nitrogen species
RONSs	Reactive oxygen and nitrogen species
ROSs	Reactive oxygen species
RSD	Relative standard deviation
SPN	Second positive system

1. Introduction

Kratom (*Mitragyna speciosa*), native of the tropical regions of Thailand, Myanmar, Malaysia, Indonesia, and other Southeast Asian countries, has gained significant recognition for its analgesic properties. This acknowledgment predominantly stems from a distinct alkaloid present in the plant known as mitragynine (MG), which is exclusive to Kratom. Consequently, the medicinal utilization of Kratom in Southeast Asia boasts a lengthy historical background. However, in recent times, Kratom has surged in popularity in Western nations, with individuals incorporating it into their routines for various health reasons, in order to address chronic pain and mood disorders. Although some nations have recently legalized the cultivation and sale of Kratom, its efficacy for these purposes remains a contentious and politically charged subject, which necessitates scientific scrutiny [1,2].

The conversion of MG into 7-hydroxymitragynine (7-OH MG) through a liver enzymatic process offers the potential for more powerful pain relief with reduced addictive properties [3–5]. This conversion, catalyzed by enzymes, represents a unique biological pathway within the human body [6]. Consequently, the efficacy of pain relief through the consumption of boiled Kratom water may be limited, as this transformation is not a common biological occurrence. Typically, extracting alkaloids from Kratom requires acidic solutions to dissolve them in water, posing challenges for subsequent applications. Following the extraction, conditions should be adjusted to an alkaline state in order to facilitate alkaloid extraction by using organic solvents. Unfortunately, this complex extraction process often results in the loss of essential compounds, leading to increased extraction costs and environmental concerns [4]. Therefore, developing a cost-effective, non-acidic organic extraction method for MG conversion holds significant promise for potential pharmaceutical applications [3–5].

Recent advancements in atmospheric-pressure plasma technology, an innovative and environmentally sustainable approach, have found applications in various fields, including food technology [7], agriculture [8–10], environmental management [11], medical treatments [12], and pharmacology [13]. The Electrical Breakdown in Liquid-phase (EBL) process is an emerging plasma technique that harnesses advanced oxidation processes (AOPs) driven by free radicals, reactive oxygen species (ROSs), reactive nitrogen species (RNSs), and reactive oxygen and nitrogen species (RONSs) in a liquid-phase environment. This results in chemically active oxidation during plasma generation [7,11,14–16]. These species play critical roles as precursors and potent oxidants with exceptionally high oxidative activity. Valuable byproducts, such as hydrogen ions (H^+), hydroxyl radicals (OH•), singlet oxygen (O•), ozone (O_3), and hydrogen peroxide (H_2O_2), are produced in this process. Furthermore, ultraviolet radiation, photons, electromagnetic waves, and x-rays, which are present during plasma generation, contribute to the unique properties of plasma [11,17–20]. Given these merits and the suitability for MG and 7-OH MG conversion, plasma presents a promising and eco-friendly solution for 7-OH MG extraction from Kratom solutions.

This research aims to address the research gap identified in previous studies concerning the complex and environmentally taxing extraction process of alkaloids from Kratom leaves. In pursuit of this objective, the study introduces the novel Electrical Breakdown in Liquid-phase (EBL) process as a potential alternative [3–6]. The primary objective of this research is to evaluate the potential of the EBL process in converting MG into 7-OH MG through advanced plasma-driven oxidation. A custom-designed plasma reactor, meticulously developed by the author, is employed to enhance plasma contact with Kratom powder during EBL. By evolving from its predecessor, the EBL reactor in Ref. [21], this innovative system has been meticulously refined in order to optimize the conversion of mitragynine into 7-hydroxymitragynine. In previous iterations, the necessity of transferring the solution outside for cooling has hindered effective plasma interaction. In order to overcome this limitation, internal cooling via a dedicated solution pipe now facilitates seamless circulation within the reactor. Furthermore, the strategic inclusion of a connecting pipe aims to maximize the interaction between the solution, Kratom powder, and plasma, thereby augmenting conversion efficiency. The primary objective of this experiment is to discern the optimal conditions for efficiently extracting 7-OH MG from Kratom leaves. Two distinct electrically driven methods (half-positive and negative half-wave voltages, potentially inducing differing corona discharge characteristics) have been employed for EBL generation, with varying processing times, in order to analyze their time-dependent effects. Subsequent to the extraction, purification procedures will be executed, and the compound structures will be confirmed through column chromatography. The quantity of extracted material will be quantified by using high-performance liquid chromatography (HPLC) techniques.

2. Experimental setup and procedure

2.1. Plasma model and experimental setup

Fig. 1 illustrates a schematic representation of the Electrical Breakdown in Liquid (EBL) process along with the experimental setup. The plasma reactor, designed in the shape of a wine Pyrex glass structure with a volume of 150 mL, features a recirculation tube on the side in order to ensure continuous plasma contact. At the midpoint, where plasma is generated, there are two tungsten pin electrodes with diameters of 0.1 mm, serving as the high-voltage and ground electrodes, strategically spaced 1 mm apart.

The Kratom solution enters the reactor through the upper solution port. At the lowest section of reactor, a gas inlet pipe aligned with its central core introduces air from the HAILEA ACO-318 air pump at a rate of 1.20 LPM, crucial for initiating plasma generation between the electrodes. In order to maintain EBL process stability, the upper reactor section controls the solution temperature within 50-55 °C. Equipped with a Kratom filter at its terminus, the upper reactor pipe conveys the solution at a constant rate of 42 mL per minute to the 5 °C cooling system via a Peristaltic Pump DP-385. Then the cooled solution is reintroduced into the reactor at its bottom for further treatment, with only 10 percent of the total solution volume extracted for cooling purposes.

The initiation of the EBL process involves connecting one end of the high-voltage electrode to a high-voltage source through a positive or negative half-wave voltage doubler (HWVD) circuit, derived from an 800 W microwave transformer. The counter electrode connects to a 50-Ω monitoring resistor in series, subsequently grounded. The maximum output voltage in this setup reaches 4.57 kV_{peak}, achieved by utilizing a 150 V_{rms} input voltage from 50 Hz variable AC power supplies [21,22].

The monitoring of the discharge voltage (V_D) and the current (I_D) electrical characteristics is conducted by using an oscilloscope (LECROY, WaveRunner 8208HD, 2 GHz, 10 GS/s). A high-voltage probe (Pintek HVP-28 H F, 75 MHz bandwidth) is employed across the plasma model, while a general-purpose passive probe (GW Instek, 100 MHz bandwidth) is connected across the monitored resistor. In order to analyze optical emission spectroscopy (OES) during plasma formation, a compact charge-coupled device (CCD) spectrometer (Newport 71SI00087) is utilized, with the optical fiber detector tip positioned 1 cm perpendicular to the electrode plane.

2.2. Kratom solution preparation and EBL treatment condition

The preparation of the Kratom leaf solution begins by selecting mature Kratom leaves from plants aged one year or older. Next, these leaves are dried at 60 °C for 24 h. Once dried, the leaves are grinded to a particle size smaller than 125 μm. Finally, 1 g of the resulting Kratom powder is combined with 100 mL of distilled water. The prepared Kratom solution will undergo treatment via the EBL process, by employing an input voltage of 150 Vrms for processing times of 5, 10, 15, 20, 40, 60, and 80 min.

2.3. Characterization of plasma-treated Kratom solution

1) Physical and chemical analysis of Kratom solution

The physical and the chemical properties of both the Kratom solution and the distilled water (serving as a reference) have been meticulously examined, by encompassing parameters such as pH, temperature, and electrical conductivity (EC). A Mettler Toledo SevenEasyTMpH meter and a Hanna HI4321 conductivity meter have been utilized to measure pH levels and EC, respectively. The solution temperature has been monitored by using a mercury thermometer submerged within the treatment solution. In order to confirm the presence of hydrogen peroxide (H_2O_2) in the solution, Quantofix peroxide 100 test strips (1–100 mg/L H_2O_2) have been employed. Additionally, the concentration of dissolved ozone in the solution has been determined by using an ozone colorimeter test kit (MColortestTM, 10 mg/L O_3).

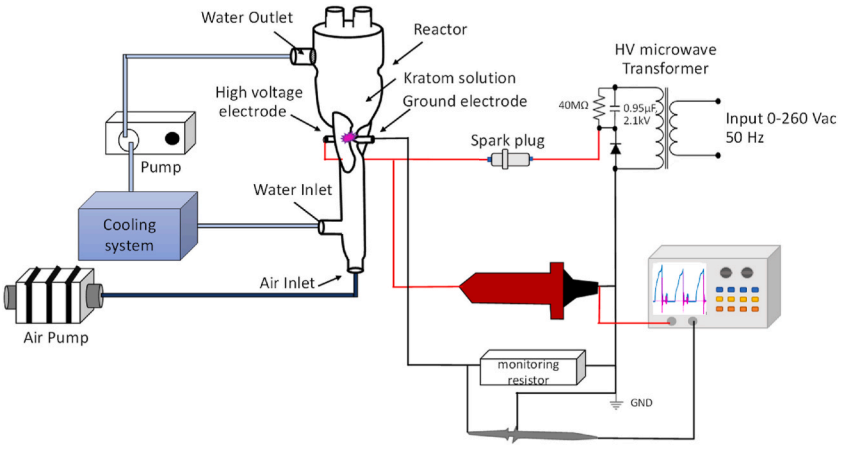

Fig. 1. A schematic illustration of the Electrical Breakdown in Liquid (EBL) process and the corresponding experimental setup.

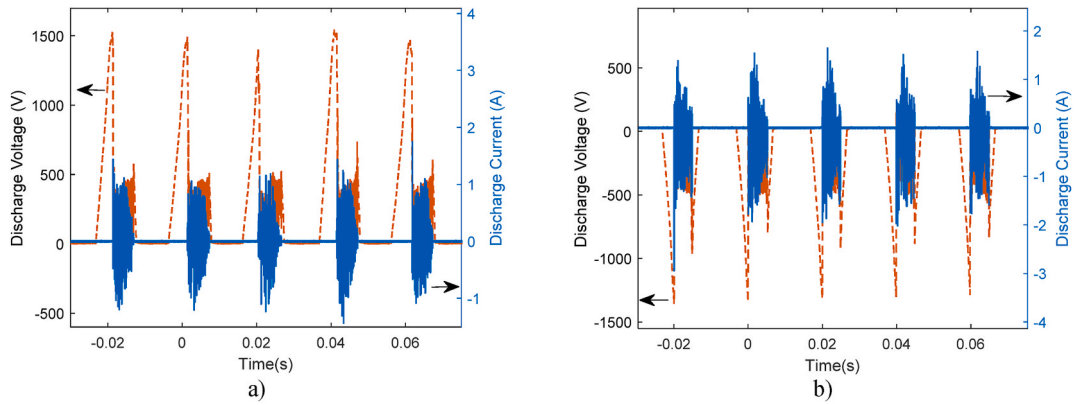

Fig. 2. Discharge voltage and current waveforms during the EBL process driven by a) positive half-wave voltage and b) negative half-wave voltage.

2) HPLC-DAD quantification of 7-hydroxymitragynine and mitragynine in Kratom solution

The HPLC system (Agilent, Santa Clara, CA, USA) has comprised the 1260 Infinity II quaternary pump, 1260 Infinity II autosampler, 1260 Infinity II multi-column thermostat, and 1260 Infinity II photodiode array detector. The separation process has occurred within an ACE 5C18-AR column (4.6 × 250 mm, 5 μm) paired with a C18 guard column. The mobile phase, consisting of acetonitrile and ammonium acetate buffer with a pH of 9.5 in a fixed ratio of 45:55, has maintained a steady flow rate of 1 mL/min. Prior to use, the mobile phase has undergone degassing and has been freshly prepared for each analysis. The detection wavelength has been consistently set at 246 nm, with an injection volume of 10 μl. All the analyses have been performed at an operating temperature of 40 °C. Under these specified chromatographic conditions, the average retention times for 7-OH-MG and MG reference standards have been determined to be 8.7 and 61.6 min, respectively. The method has undergone validation in a Kratom solution, following the guidelines established by the International Conference on Harmonization (ICH), in order to assess linearity, selectivity, accuracy, precision, limit of detection (LOD), and limit of quantification (LOQ) [23].

2.4. Statistical analysis

All the experimental conditions and measurements have undergone rigorous validation through triplicate testing to derive the mean result value. Statistical analyses have been conducted by using *t*-test analysis and one-way analysis of variance (ANOVA) in order to identify significant differences among samples at a significance level of $p < 0.05$.

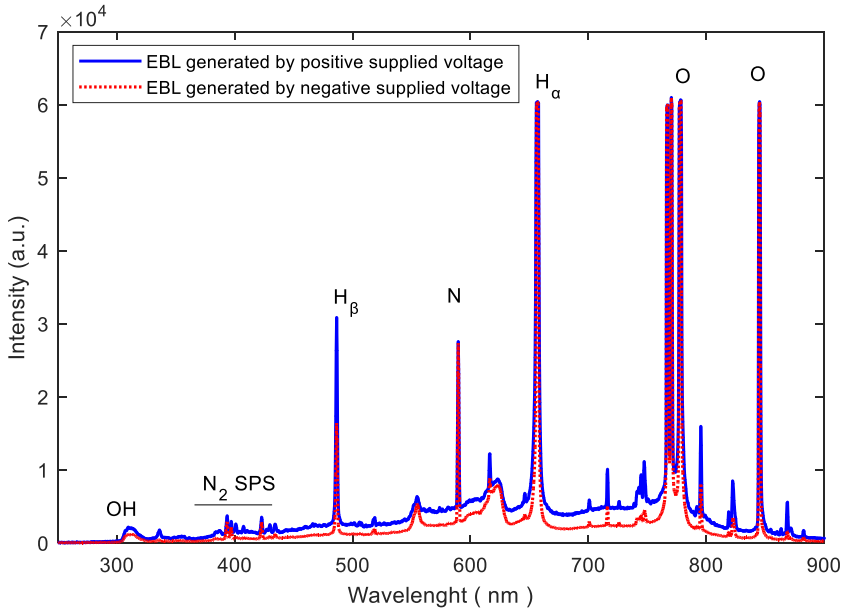

Fig. 3. Optical emission spectra (OES) in the Kratom solution during the EBL process generated by positive and negative half-wave supplied voltages.

Table 1
Quantities of MG and 7-OH-MG in Kratom solution at various EBL processing durations*.

Time (min.)	Mean concentration ± SD (μg/mL), n = 3			Productivity of 7-OH-MG (%)	7-OH-MG content (μg/g of dried weight of Kratom leaves)
	7-OH-MG	7-OH-MG production	MG		
EBL processing generated by POSITIVE half-wave supplied voltage (PV-EBL)					
0	9.03 ± 0.43	0.00	36.19 ± 2.24	0.00	9.03 ± 0.43
5	13.69 ± 1.96	4.66 ± 0.67	33.89 ± 0.70	12.88 ± 1.84	13.69 ± 1.96
10	17.16 ± 1.12	8.13 ± 0.53	30.89 ± 0.94	22.46 ± 1.46	17.16 ± 1.12
15	21.07 ± 1.37	12.04 ± 0.78	29.36 ± 2.87	33.27 ± 2.16	21.07 ± 1.37
20	24.85 ± 1.34	15.81 ± 0.85	23.31 ± 0.98	43.70 ± 2.36	24.85 ± 1.34
40	15.86 ± 1.67	6.82 ± 0.72	0.00	18.86 ± 1.99	15.86 ± 1.67
60	7.35 ± 0.52	−1.68 ± 0.12	0.00	−4.66 ± 0.33	7.35 ± 0.52
80	3.68 ± 0.58	−5.36 ± 0.84	0.00	−14.80 ± 2.32	3.68 ± 0.58
EBL processing generated by NEGATIVE half-wave supplied voltage (NV-EBL)					
0	9.03 ± 0.43	0.00	36.19 ± 2.24	0.00	9.03 ± 0.43
5	9.65 ± 0.66	0.62 ± 0.04	32.33 ± 1.99	1.71 ± 0.12	9.65 ± 0.66
10	10.50 ± 0.44	1.47 ± 0.06	29.25 ± 1.68	4.05 ± 0.17	10.50 ± 0.44
15	11.03 ± 0.25	1.99 ± 0.05	25.90 ± 2.43	5.52 ± 0.12	11.03 ± 0.25
20	11.88 ± 0.57	2.85 ± 0.14	22.56 ± 2.97	7.88 ± 0.38	11.88 ± 0.57
40	6.42 ± 0.56	−2.62 ± 0.23	0.00	−7.22 ± 0.63	6.42 ± 0.56
60	2.41 ± 0.43	−6.62 ± 1.18	0.00	−18.30 ± 3.26	2.41 ± 0.43
80	0.00	−9.03 ± 0.00	0.00	−24.96 ± 0.00	0.00

* Regarding the *t*-test analysis and one-way ANOVA conducted at a significance level of $p < 0.05$, all the data show significant differences across all the dimensions, including treatment times and supplied voltage polarities.

3. Experimental results and discussion

3.1. Electrical characteristics of the EBL processing

The electrical characteristics of discharge voltage and current waveforms under different electrically driven methods during the EBL process are illustrated in Fig. 2. In this work, the positive and the negative half-wave supplied voltage (PV and NV) have been utilized for EBL process generation. Under no-load conditions, the electrodes have been supplied at the input voltage of 150 V_{rms}, resulting in an absolute output voltage across electrodes of approximately 4.48 kV_{peak}.

Regarding Fig. 2, it could be noticed that the positive discharge case (Fig. 2a)) has slightly higher pulse amplitudes, while the negative discharge case (Fig. 2b)) has slightly lower amplitudes of inception voltage with higher repetition rates of discharge current, called Trichel pulses [24–27]. The absolute peak voltages at the breakdown points of PV case are in the range of 1.40-1.52 kV slightly higher than the ones of the NV case, which are 1.32-1.37 kV. The rms of discharge voltage and currents are 477.10 V and 41.30 mA, and 331.1 V and 49.6 mA for PV and NV cases, respectively. The detailed electrical characteristics of EBL process can be found in Ref. [21].

3.2. Characteristics of the optical emission spectrum during EBL processing

During the EBL process, optical emission spectra (OES) have been examined to gain insights into the chemical reactions occurring. Fig. 3 illustrates the comparative OES plots during the EBL process of the Kratom solution under positive and negative half-wave supplied voltages (PV and NV). Both conditions exhibit similar OES patterns but with varying magnitudes. Consistent observations from both conditions include the presence of highly reactive OH• species at 309.6 nm. Additionally, atomic oxygen emissions are detected at wavelengths of 777.4 nm and 844 nm. The N_2 second positive system (SPN) is evident in the range from 310 nm to 400 nm. Notably, spectral lines for H_β, atomic nitrogen (N), and Hα appear at 486.13, 589.72, and 656.28 nm, respectively. In the realm of Advanced Oxidation Processes (AOPs), these radical species play a pivotal role as potent agents that initiate oxidation. Their involvement extends beyond mere reactivity, actively contributing to the creation of beneficial synergistic reactive oxygen and nitrogen species (RONSs) [28–34]. The chemical reactions observed during the EBL process, as related to the observed peaks, are listed in Table 2 [35–37]. Regarding Fig. 3, it can be noticed that the magnitude of the broad spectrum is more significant in the PV condition. This broad spectrum is attributed to black-body radiation resulting from joule heating during spark discharge, potentially originating from molecular bands such as N_2 bands commonly observed in air discharges [38–41].

3.3. Characteristics of treated Kratom solution and 7-hydroxymitragynine conversion after EBL processing

In this study, the physical-chemical characteristics of both treated DI water and Kratom solution have been examined during the 0–20 min duration of the EBL process, as depicted in Fig. 4. Notably, as the treatment time of the EBL process has increased, the electrical conductivity (EC), hydrogen peroxide (H_2O_2), and dissolved ozone (O_3) concentrations have increased, while the pH (Fig. 4a)) has exhibited the opposite trend for both EBL processes generated by positive and negative half-wave supplied voltages (PV-

Table 2
Chemical reactions during EBL process [35–37].

Reactive species	Chemical reactions
Hydrogen ion (H^+), Hydrogen radical (H•), Hydroxyl radical (OH•), and Hydroxide (OH^-)	$H_2O + e^- \rightarrow OH\bullet + H\bullet + e^-$
	$H_2O + e^- \rightarrow H+ + OH\bullet + 2e^-$
	$H_2O + e^- \rightarrow H\bullet + O\bullet + H\bullet + e^-$
	$H_2O + M^* \rightarrow OH\bullet + H\bullet + M$
	$H_2O + UV \rightarrow H_2O^*$
	$H_2O^* + UV \rightarrow H^+ + OH^-$
	$OH^- \rightarrow OH\bullet + e^-$
	$H_2O_2 + h\nu \rightarrow OH\bullet + OH\bullet$
Atomic oxygen (O), Oxygen ion (O^+), Singlet oxygen ($^1O_2$), and Superoxide ($O_2{}^{*-}$)	$O_2 + e^- \rightarrow O^+ + O + 2e^-$
	$O_2 + e^- \rightarrow O^- + O$
	$O_2 + M^* \rightarrow 2O + M$
	$O_2 + H\bullet \rightarrow OH\bullet + O$
	$O_2 + e^- \rightarrow {}^1O_2$
	$O + O \rightarrow {}^1O_2$
	$O_2 + e^- \rightarrow O_2{}^{*-}$
	$OH\bullet + HO_2 \rightarrow O_2{}^{*-} + H_2O$
Hydrogen peroxide (H_2O_2)	$OH\bullet + OH\bullet \rightarrow H_2O_2$
Ozone (O_3)	$O + O_2 \rightarrow O_3$
Excited Nitrogen (N)	$N_2 + e^- \rightarrow N_2^* + e^-$
	$N_2 + e^- \rightarrow N + N$
	$N_2 + O_2{}^{*-} \rightarrow O_2 + N + N$
Nitric oxide (NO)	$N + O_2 \rightarrow NO + O$
	$N_2 + O \rightarrow NO + N$
	$NO_2 + O \rightarrow NO + O_2$
	$NO_2 + h\nu \rightarrow NO + O\bullet$
	$NO_3 + h\nu \rightarrow NO + O_2$
Nitrate (NO_2) and Nitrous acid (HNO_2)	$NO + O_3 \rightarrow NO_2 + O_2$
	$2NO + O_2 \rightarrow 2NO_2$
	$NO + OH\bullet \rightarrow HNO_2$
	$HNO_2 + OH\bullet \rightarrow NO_2 + H_2O$
Nitrite (NO_3), Nitric acid (HNO_3), Peroxynitrate ($ONOO^-$), and Peroxynitrous acid (ONOOH)	$NO_2 + O\bullet \rightarrow NO_3$
	$NO_2 + OH\bullet \rightarrow HNO_3$
	$2NO_2 + H_2O \rightarrow NO_2^- + NO_3^- + 2H^+$
	$3NO_2 + H_2O \rightarrow 2HNO_3 + NO$
	$NO_2^- + O_3 \rightarrow NO_3^- + O_2$
	$NO_2^- + H_2O_2 + H^+ \rightarrow ONOOH + H_2O$
	$NO_2 + OH\bullet \rightarrow ONOOH \rightarrow ONOO^- + H^+$
	$ONOOH \rightarrow NO_3^- + H^+$
	$O_2{}^{*-} + NO \rightarrow ONOO^-$

Where M and M* are neutral gas molecule and its excited state.

and NV- EBL).

The significant increase in EC of the plasma-treated Kratom solution illustrated in Fig. 4b) can be attributed to the abundant active ions generated during the EBL process [35,42–46]. Initially, the EC values of DI water and Kratom solution have been approximately 0.81 ± 0.02 and 716.47 ± 7.05 μS/cm, respectively. It is observed that the EC values of the PV-EBL case for both DI water and Kratom solution are slightly higher than those of the NV-EBL case. After 20 min of the EBL process, the EC values of the PV-EBL case for DI water and Kratom solution have increased by 342.18 and 1.40 times their initial values, respectively, and have been 1.17 and 1.13 times higher compared to the ones of the NV-EBL case after the same duration.

During and after the EBL process, various compounds, including H_2O_2, nitric acid (HNO_3), peroxynitrous acid (ONOOH), and others, have been formed, resulting in a decrease in pH levels. While the initial pH of DI water has been around 6.86 ± 0.07, when mixed with Kratom powder, it has decreased to 4.80 ± 0.24, indicating the slight acidity of the Kratom powder due to phenolic acids [47]. Subsequently, as shown in Fig. 2b), the pH of all the cases has decreased to around 3.18–4.25. The lowest pH has been observed in the Kratom solution subjected to PV-EBL, at 3.18 ± 0.19.

Concerning the concentration of dissolved H_2O_2 in the plasma-treated solution, it has been observed that the H_2O_2 concentration has increased over time, nearly reaching 100 mg/L, the upper limit of the strip, in the case of Kratom solution subjected to both PV- and NV-EBL processing, as illustrated in Fig. 4c). The H_2O_2 concentration in plasma-treated Kratom solutions has been higher than that in plasma-treated DI water. Notably, in the PV-EBL cases, the H_2O_2 concentration has been higher than that in the NV-EBL cases.

Fig. 4d) illustrates the concentration of dissolved O_3 in the solution. It can be noticed that the O_3 concentration in both cases of DI water has increased rapidly, exceeding 10 mg/L (the limit of the testing kit) within the first 10 min after the EBL process. Conversely, for the Kratom solution subjected to PV- and NV-EBL processing, the O_3 concentration has gradually increased to around 7 and 2.7 mg/L, respectively.

It is important to note that the assessment of H_2O_2 and O_3 concentrations has relied on a color-based testing method, with human observers providing their judgments. When values have not aligned precisely with the scale indicated on the test kit label, they have

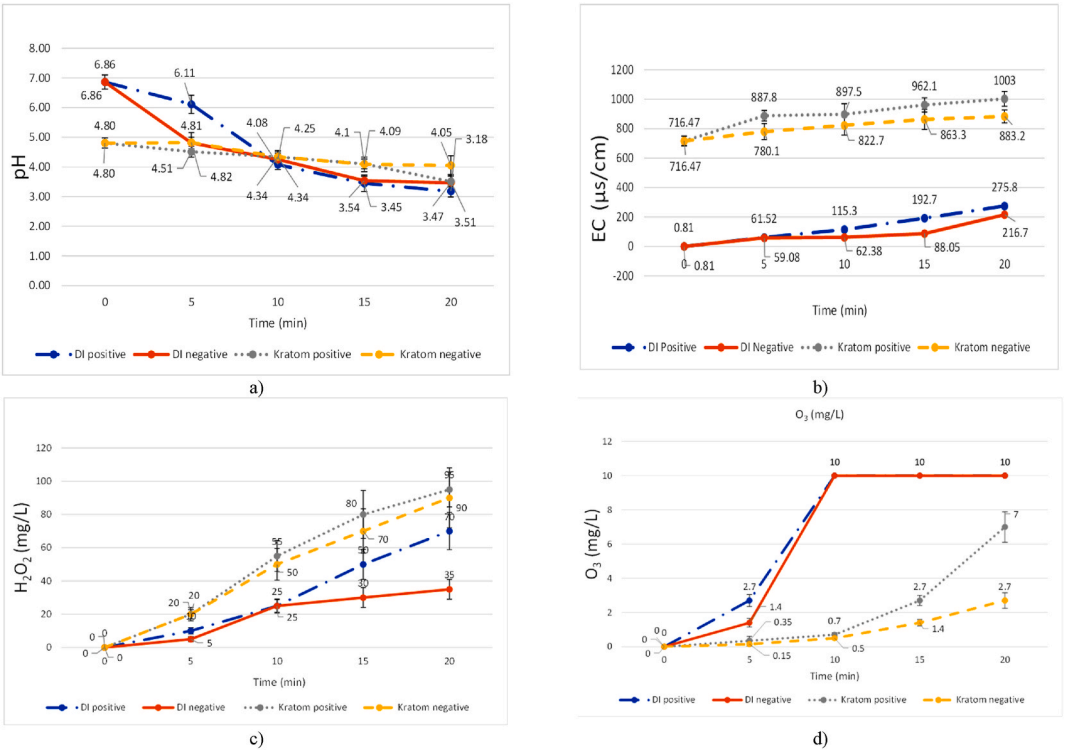

Fig. 4. Kratom solution characteristics under different supplied voltage polarities (positive and negative half-wave voltage), depicted as: a) Electrical Conductivity (EC), b) pH, c) Hydrogen Peroxide (H_2O_2), and d) Ozone (O_3).

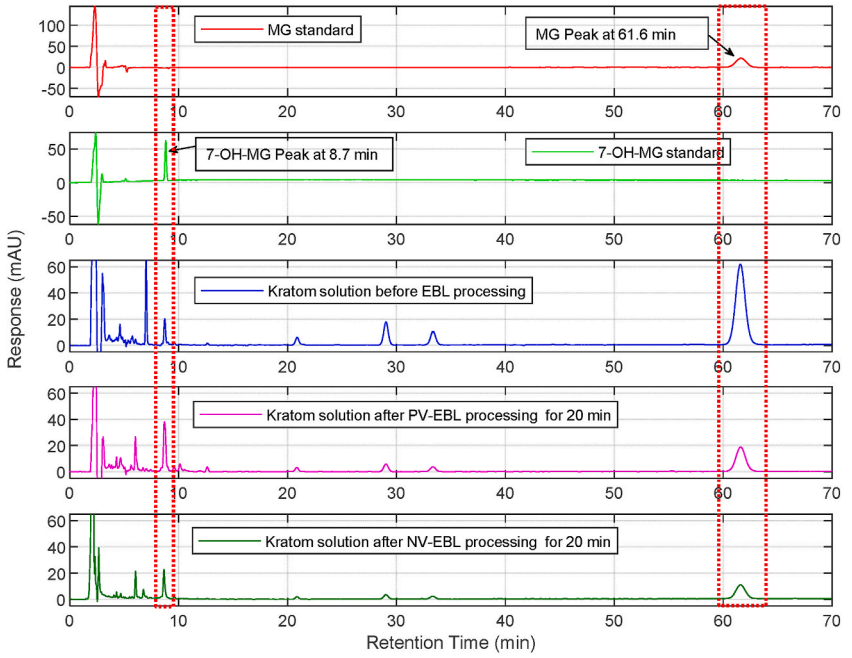

Fig. 5. Chromatograms of MG standard, 7-OH-MG standard, Kratom solution before EBL processing, and Kratom solution after PV- and NV-EBL processing for 20 min, obtained by HPLC-DAD at 246 nm.

been considered indicative of concentrations approximated by comparing the observed color with the reference color range, employing a color interpolation approach.

3.4. Validation of HPLC method for the determination of 7-hydroxymitragynine and mitragynine in Kratom solutions

This study has focused on validating a high-performance liquid chromatography (HPLC) methodology for quantifying 7-Hydroxymitragynine (7-OH-MG) and Mitragynine (MG) in Kratom solutions. The developed HPLC system has demonstrated exceptional specificity in detecting 7-OH-MG and MG, with mean retention times of 8.7 and 61.6 min, respectively, as depicted in Fig. 5. All the other analytical parameters have met the established standards.

The analytical range for 7-OH-MG has ranged from 5 to 30 μg/mL, exhibiting high linearity (r^2 = 0.9998), a limit of detection (LOD) of 0.1 μg/mL, and a limit of quantification (LOQ) of 0.5 μg/mL. Similarly, for MG, the analytical range has been 10–60 μg/mL, with notable linearity (r^2 = 0.9999), an LOD of 0.2 μg/mL, and an LOQ of 0.5 μg/mL. Method precision has been rigorously evaluated, with both repeatability (intra-day) and intermediate precision (inter-day) showing relative standard deviation (RSD) values consistently below 2 % (ranging from 0.96 % to 1.82 %), indicating exceptional precision.

Accuracy has been assessed by analyzing the recovery of spiked 7-OH-MG and MG in Kratom solutions and comparing the measured values with the actual concentrations. The method has exhibited robust recovery rates ranging from 97.24 % to 102.86 %. Thus, the HPLC method has demonstrated reliability in quantifying 7-OH-MG and MG in Kratom solutions, making it suitable for analytical applications in this context.

3.5. Mitragynine conversion and 7-hydroxymitragynine production after EBL process

In the context of validating the method for analyzing Kratom solutions, the validation process has involved examining the contents of both 7-OH-MG and MG before and after the EBL process, as illustrated in Fig. 5. As indicated in Table 1, the initial concentrations of MG and 7-OH-MG have been quantified at 36.19 ± 2.24 μg/mL and 9.03 ± 0.43 μg/mL, respectively.

In order to evaluate the production of 7-OH-MG, the post-plasma treatment concentration has been subtracted from the initial concentration. Then, productivity has been determined by calculating the ratio of 7-OH-MG production to the initial MG concentration, which has been multiplied by 100. Notably, the highest 7-OH-MG productivity, reaching 43.70 ± 2.36 %, has been achieved after subjecting the Kratom solution to a 20-min plasma treatment. Additionally, the highest concentration of 7-OH-MG quantified has been 2,485 ± 134 μg/g of dried Kratom leaves weight. Further experimental results, including the relationship between MG and 7-OH-MG concentrations at different EBL processing times, are presented in Table 1 and Fig. 6, respectively. It is important to note that comprehensive statistical analyses, including *t*-test and one-way ANOVA with a significance level set at $p < 0.05$, have revealed significant differences across all dimensions, including treatment times and supplied voltage polarities, indicating a comprehensive differentiation in the data.

As depicted in Fig. 6, the MG concentration in both Kratom solutions subjected to EBL processing generated by positive half-wave and negative half-wave supplied voltage (PV- and NV- EBL) cases exhibits a decreasing trend with increasing concentrations of 7-OH-MG. However, after 40 min of EBL processing, the MG concentration has vanished in both cases, while the concentration of 7-OH-MG has decreased at a slower rate compared to its conversion to MG. It is important to note that due to operational limitations associated with the power supply duration, the EBL process has been originally constrained to a maximum duration of 20 min. Consequently, efforts have

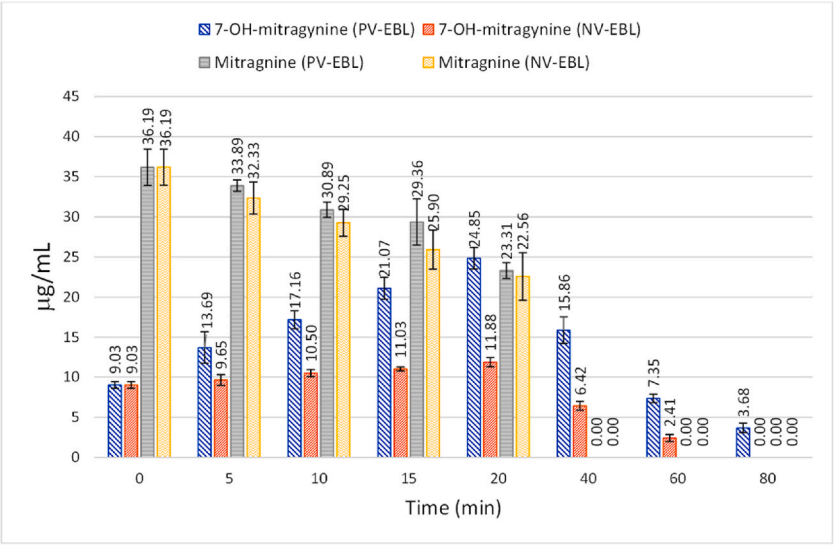

Fig. 6. Concentrations of MG and 7-OH-MG at different EBL processing times under "PV-EBL" and "NV-EBL" conditions, representing positive and negative half-wave supplied voltages, respectively.

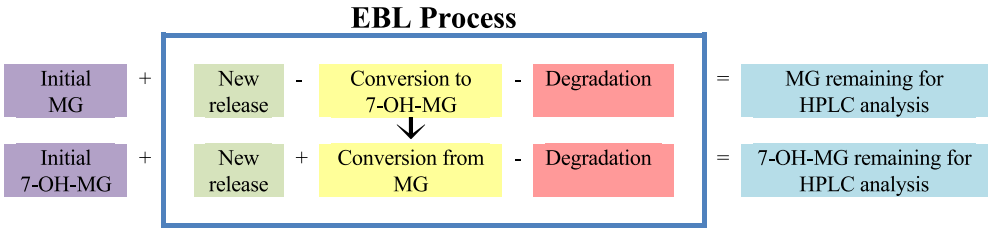

Fig. 7. Impact of the EBL process on MG and 7-OH-MG contents in the sample solution.

been made to extend the operational time limit of the power supply in subsequent experiments, encompassing treatment durations of 5, 10, 15, and 20 min. As a result, the examination of MG and 7-OH-MG contents at prolonged operational intervals of 40, 60, and 80 min has been undertaken, by using the 20-min EBL-treated solution for the second, the third, and the fourth iterations of the EBL process, respectively. However, it can be noticed that the conversion of 7-OH-MG has been significantly suppressed and ultimately ceased, as demonstrated in Fig. 6. The underlying causes of this phenomenon remain a topic of ongoing research. Nonetheless, it is important to note that this specific observation holds potential implications for future studies in this field.

Regarding the presence of both 7-OH-MG and MG contents in the Kratom solution before and after the EBL process, as well as the data provided in Table 1, Fig. 7 offers insight into this phenomenon. In the sample solution, the MG content comprises the fraction initially dissolved in water before entering the EBL process, the amount subsequently released during the EBL process, and a portion transformed into 7-OH-MG and related compounds. Similarly, the 7-OH-MG content in the sample solution includes the 7-OH-MG initially dissolved in water before the EBL process, the quantity liberated during the EBL process, the portion that increases due to the transformation of MG, and a specific amount lost as it converts into other substances.

3.6. Influence of EBL process on mitragynine to 7-hydroxymitragynine conversion

In this research, the Electrical Breakdown in Liquid-phase (EBL) process has been employed to convert mitragynine (MG) into 7-hydroxymitragynine (7-OH MG). The breakdown mechanism within liquid electrical discharges is a complex process involving various phases and the generation of multiple reactive species. The intricacy is attributed to the unique characteristics of liquid media and it is further influenced by factors like electrode geometry, voltage properties, and liquid purity. This complexity characterizes the breakdown in liquids and is exemplified by the gas bubble theory and in-bubble contacted discharge in the EBL process. The cycle of discharge in the EBL system can be briefly elucidated as follows. The pre-breakdown phase is initiated by the corona streamer discharge, which generates small gas bubbles through the heating of highly stressed electrode tips in the liquid. Over time, the streamer evolves into a plasma column, triggering a spark streamer discharge when an air bubble, released from the gas inlet at the lowest section of the reactor, approaches closely. The discharge within the air bubbles expands due to the non-uniform distribution of the electric field. The cycle concludes as the air bubble undergoes a change in shape and traverses the electrode gap. This sequence initiates a new cycle in the process [21,42,48–51].

Generally, the conversion of MG to 7-OH MG likely involves several key factors. Firstly, it necessitates the provision of acidic conditions. Furthermore, the transformation of MG into 7-OH MG involves an oxidation reaction catalyzed by an enzyme. This catalysis process [4,52] is closely associated with the generation of plasma in the presence of air, giving rise to protons, electrons, ions, and plenty of free radicals, most notably oxygen free radicals, nitrogen free radicals, as well as reactive oxygen species (ROSs), reactive nitrogen species (RNSs), and reactive oxygen and nitrogen species (RONS). These components play a pivotal role, functioning as precursors and potent oxidizing agents.

This intricate chemical interplay leads to the creation of valuable byproducts integral to the Advanced Oxidation Processes (AOPs). These byproducts include hydrogen ions (H^+), hydroxyl radicals (·OH), singlet oxygen (·O), ozone (O_3), and hydrogen peroxide (H_2O_2) [17–19]. Some of the essential chemical reactions during the EBL process can be seen in Table 2. Hence, the efficiency of plasma under atmospheric conditions for alkaloid extraction and the conversion of MG to 7-OH MG in Kratom leaves is rooted in a conceptual framework. The concept posits that plasma stimulation of Kratom leaves facilitates the dispersion of protons and free radicals generated during plasma formation throughout the tissue surface and into the fiber of the Kratom powder. These protons make the solution acidic, causing the ionization of alkaloids and rendering them soluble in water because the dissociation constant (pKa) of MG conjugate acid is approximately 8.11 [53]. Simultaneously, the generated free radicals interact with MG components, triggering oxidation reactions that result in the conversion of MG derivatives into 7-OH MG [4,6,17–19,54–56].

By analyzing the experimental results depicted in Fig. 6, a compelling trend has emerged within the EBL processing generated by a positive half-wave supplied voltage case. It can be noticed that as the experimental duration extended, there has been a notable decline in the MG substance, coinciding with a concurrent increase in the abundance of 7-OH-MG. Notably, extending the EBL processing time to 20 min has facilitated the most enhanced modifications in MG. A comparative evaluation of 7-OH-MG production from the EBL processing generated by the positive half-wave and the negative half-wave supplied voltage (PV- and NV-EBL) cases unveiled a distinct contrast in their effectiveness in augmenting substances. Remarkably, in the PV-EBL case, the enhancement has been 2.09 times greater than the NV-EBL case after a 20-min EBL process. These findings underscore the consistent superiority of the PV-EBL case over its negative counterpart. The disparity in performance is likely attributed to the reduced production of ozone-free radicals in the

NV-EBL case as shown in Fig. 4d), signifying a less pronounced impact of plasma in this context.

Concerning the experimental findings depicted in Fig. 4d), it can be noticed that the O_3 concentration in plasma-treated Kratom solutions is notably lower when compared to plasma-treated DI water, in both PV- and NV-EBL cases. This observation aligns consistently with the conversion rate of MG to 7-OH MG in the PV case, as opposed to the NV-EBL case. Consequently, it is reasonable to infer that O_3 plays a significant role in the conversion of MG to 7-OH MG. Additionally, ultraviolet rays, shock waves, and photons produced during plasma generation may further contribute to the synergistic stimulation of chemical reactions within Kratom leaves [16,28–34,57].

The hypothetical mechanism of converting mitragynine (MG) into 7-hydroxymitragynine (7-OH-MG) through the EBL process in this study can be elucidated as depicted in Fig. 8. The environment created by the EBL process, including the presence of reactive oxygen species, acidity, and heat, plays a pivotal role in this transformation mechanism. This process consists of three essential steps, as follows. (1) Formation of epoxide: MG, an intrinsic indole alkaloid, exhibits the oxidation potential when exposed to reactive oxygen species. The theoretical framework for this indole oxidation mechanism begins with the electrophilic addition of reactive oxygen species to the carbon-carbon double bond, giving rise to an intermediate epoxide of considerable instability [58,59]. (2) Formation of alcohol from epoxide: in an acidic environment, the epoxide accepts a proton, making the carbon at position 2 more electrophilic. Furthermore, the carbon at position 2 is also surrounded by highly electronegative atoms, such as oxygen and nitrogen, which further increase its electrophilic nature. This electron deficiency renders it receptive to nucleophilic substitution reactions, primarily initiated by the presence of the hydroxyl group (OH). The leaving group is the oxygen atom of the epoxide in the form of the alkoxide, which is converted to alcohol during an acidic workup. As a consequence of these reactions, the cascade leads to the formation of 2,7-dihydroxymitragynine [60,61]. (3) In an acidic condition, and with heat generated by plasma stimulation, water loss occurs at the tertiary alcohol at position 2 of the 2,7-dihydroxymitragynine molecule, resulting in the final product, 7-hydroxymitragynine [62,63].

The research findings presented herein not only contribute to a deeper scientific understanding of alkaloid conversion within Kratom leaves but also hold promise for practical applications in healthcare, pharmaceuticals, and sustainable technologies. The EBL process emerges as a novel technique for 7-OH-MG conversion, demonstrating considerable potential for further exploration. However, it is important to acknowledge areas for improvement. Initially, the EBL process has been limited to a maximum duration of 20 min due to constraints related to power supply duration. Attempts to extend this duration have resulted in a notable suppression of 7-OH-MG conversion, warranting ongoing investigation into the underlying causes. Nevertheless, this observation underscores the need for careful consideration in future research endeavors within this domain. This study represents a significant step forward in unlocking the potential of natural resources to advance medical science while promoting environmental sustainability.

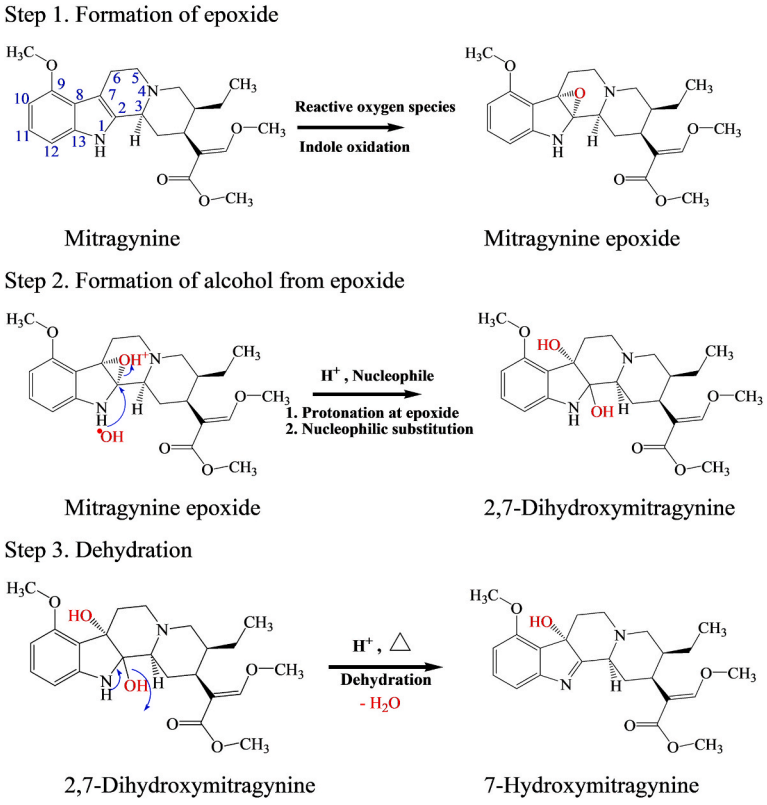

Fig. 8. Proposed mechanism for the conversion of mitragynine to 7-hydroxymitragynine via the EBL process.

4. Conclusion

This research explores the impact of the Electrical Breakdown in Liquid-phase (EBL) process on the conversion of mitragynine (MG) in Kratom leaves to 7-hydroxy mitragynine (7-OH-MG) through advanced oxidation processes (AOPs). In order to enhance plasma exposure to Kratom leaf powdered solutions during EBL, a novel reactor is utilized, incorporating both positive and negative half-wave supplied voltages (PV and NV). The findings indicate that the PV-EBL case outperforms the NV-EBL case in transforming MG into 7-OH-MG, with the highest yield achieved after 20 min of EBL due to its greater production of ozone and free radicals. Ozone, ROSs, RNSs, RONSs, and other plasma-induced factors significantly influence this conversion. These results lay the groundwork for the advancement of methodologies for the production of 7-OH-MG from Kratom leaves, offering potential applications in pharmacology and medical research. The proposed mechanism for this conversion involves epoxide formation, succeeded by the creation of alcohol from the epoxide, ultimately resulting in the production of 7-OH-MG, underscoring the role of plasma-induced factors in this process.

Data availability

Data included in article/supp. material/referenced in article.

CRediT authorship contribution statement

Weerasak Samee: Writing – review & editing, Writing – original draft, Visualization, Supervision, Resources, Methodology, Formal analysis, Conceptualization. **Khanit Matra:** Writing – review & editing, Writing – original draft, Visualization, Validation, Supervision, Resources, Project administration, Methodology, Investigation, Formal analysis, Conceptualization. **Nattawut Lakkham:** Investigation. **Beelawan Dongkaew:** Investigation. **Passakorn Sumkhum:** Investigation. **Wutthichok Sangwang:** Visualization, Investigation. **Wasin Nupangtha:** Validation, Investigation. **Jiraporn Promping:** Validation, Investigation.

Declaration of generative AI and AI-assisted technologies in the writing process

During the preparation of this work, the authors used ChatGPT [chat.openai.com] in order to improve language and readability. After using this tool/service, the authors reviewed and edited the content as needed and take full responsibility for the content of the publication.

Acknowledgment

This research was supported by the Faculty of Engineering, Srinakharinwirot University, Thailand through a grant derived from faculty income for the fiscal year 2022. Appreciation is also extended to Srinakharinwirot University and the Thailand Institute of Nuclear Technology (TINT), Thailand for their invaluable support.

References

[1] D.A. Todd, et al., Chemical composition and biological effects of kratom (Mitragyna speciosa): in vitro studies with implications for efficacy and drug interactions, Sci. Rep. 10 (1) (Nov. 2020) 19158, https://doi.org/10.1038/s41598-020-76119-w.
[2] C. Veltri, O. Grundmann, Current perspectives on the impact of Kratom use, Subst. Abuse Rehabil. 10 (Jul. 2019) 23–31, https://doi.org/10.2147/SAR.S164261.
[3] S.C. Eastlack, E.M. Cornett, A.D. Kaye, Kratom—pharmacology, clinical implications, and outlook: a comprehensive review, Pain Ther 9 (1) (Jun. 2020) 55–69, https://doi.org/10.1007/s40122-020-00151-x.
[4] A.C. Kruegel, et al., 7-Hydroxymitragynine is an active metabolite of mitragynine and a key mediator of its analgesic effects, ACS Cent. Sci. 5 (6) (Jun. 2019) 992–1001, https://doi.org/10.1021/acscentsci.9b00141.
[5] S. Chakraborty, et al., Kratom alkaloids as probes for opioid receptor function: pharmacological characterization of minor indole and oxindole alkaloids from kratom, ACS Chem. Neurosci. 12 (14) (Jul. 2021) 2661–2678, https://doi.org/10.1021/acschemneuro.1c00149.
[6] M. Zhao, et al., Cytochrome P450 enzymes and drug metabolism in humans, Int. J. Mol. Sci. 22 (23) (Nov. 2021) 12808, https://doi.org/10.3390/ijms222312808.
[7] I. Prasertsung, K. Aroonraj, K. Kamwilaisak, N. Saito, S. Damrongsakkul, Production of reducing sugar from cassava starch waste (CSW) using solution plasma process (SPP), Carbohydr. Polym. 205 (2019) 472–479, https://doi.org/10.1016/j.carbpol.2018.10.090. July 2018.
[8] K. Matra, Y. Tanakaran, V. Luang-In, S. Theepharaksapan, Enhancement of lettuce growth by PAW spray gliding arc plasma generator, IEEE Trans. Plasma Sci. 50 (6) (Jun. 2022) 1430–1439, https://doi.org/10.1109/TPS.2021.3105733.
[9] W. Seelarat, et al., Enhanced fruiting body production and bioactive phytochemicals from white cordyceps militaris by blending cordyceps militaris and using cold plasma jet, Plasma Chem. Plasma Process. 43 (1) (Jan. 2023) 139–162, https://doi.org/10.1007/s11090-022-10292-w.
[10] S. Theepharaksapan, et al., The potential of plasma-activated water as a liquid nitrogen fertilizer for microalgae cultivation, IEEE Trans. Plasma Sci. (2024) 1–11, https://doi.org/10.1109/TPS.2024.3362629.
[11] S. Theepharaksapan, K. Matra, Atmospheric argon plasma jet for post-treatment of biotreated landfill leachate, in: iEECON 2018 - 6th International Electrical Engineering Congress, 2018, https://doi.org/10.1109/IEECON.2018.8712320.
[12] A. Filipić, I. Gutierrez-Aguirre, G. Primc, M. Mozetič, D. Dobnik, Cold plasma, a new hope in the field of virus inactivation, Trends Biotechnol. 38 (11) (Nov. 2020) 1278–1291, https://doi.org/10.1016/j.tibtech.2020.04.003.
[13] L. Gao, X. Shi, X. Wu, Applications and challenges of low temperature plasma in pharmaceutical field, J. Pharm. Anal. 11 (1) (2021) 28–36, https://doi.org/10.1016/j.jpha.2020.05.001.
[14] F. Ma, et al., Effect of solution plasma process with bubbling gas on physicochemical properties of chitosan, Int. J. Biol. Macromol. 98 (2017) 201–207, https://doi.org/10.1016/j.ijbiomac.2017.01.049.
[15] O. Takai, Solution plasma processing (SPP), Pure Appl. Chem. 80 (9) (2008) 2003–2011, https://doi.org/10.1351/pac200880092003.
[16] S. Sangwanna, et al., Air atmospheric pressure plasma jet to improve fruiting body production and enhance bioactive phytochemicals from mutant cordyceps militaris (white cordyceps militaris), Food Bioprocess Technol. (123456789) (2023), https://doi.org/10.1007/s11947-023-03028-x.

[17] R. Brandenburg, Dielectric barrier discharges: progress on plasma sources and on the understanding of regimes and single filaments, Plasma Sources Sci. Technol. 26 (5) (2017) 053001, https://doi.org/10.1088/1361-6595/aa6426.
[18] A. Yehia, The electrical characteristics of the dielectric barrier discharges, Phys. Plasmas 23 (6) (2016), https://doi.org/10.1063/1.4954300.
[19] V. Nehra, A. Kumar, H. Dwivedi, Atmospheric non-thermal plasma sources, Int. J. Eng. 2 (1) (2008) 53–68.
[20] Y. Tanakaran, K. Matra, The influence of atmospheric non-thermal plasma on jasmine rice seed enhancements, J. Plant Growth Regul. 41 (1) (Jan. 2022) 178–187, https://doi.org/10.1007/s00344-020-10275-1.
[21] K. Matra, et al., Application of electrical breakdown in liquid process on inulin structural transformations, IEEE Access 11 (June) (2023) 114777–114789, https://doi.org/10.1109/ACCESS.2023.3321339.
[22] C. Dechthummarong, K. Matra, An investigation of plasma activated water generated by 50 Hz half wave AC high voltage, in: iEECON 2018 - 6th International Electrical Engineering Congress, 2018, https://doi.org/10.1109/IEECON.2018.8712312.
[23] P. Borman, D. Elder, Q2(R1) validation of analytical procedures, in: ICH Quality Guidelines, Wiley, 2017, pp. 127–166.
[24] K. Matra, Y. Tanakaran, T. Temponsub, S. Nimbua, P. Thab-In, C. Pluksa, Electrical characteristics of atmospheric air corona plasma by multi-pin electrodes, Int. Rev. Electr. Eng. 14 (3) (Jun. 2019) 226–236, https://doi.org/10.15866/iree.v14i3.16726.
[25] H. Ait Said, H. Nouri, Y. Zebboudj, Effect of air flow on corona discharge in wire-to-plate electrostatic precipitator, J. Electrost. 73 (Feb. 2015) 19–25, https://doi.org/10.1016/j.elstat.2014.10.004.
[26] M. Liu, J. Tang, Q. Yao, Y. Miao, Development processes of positive and negative DC corona under needle-plate electrode in air, in: 2016 IEEE International Conference on High Voltage Engineering and Application, ICHVE), Sep. 2016, pp. 1–4, https://doi.org/10.1109/ICHVE.2016.7800827.
[27] T. Stegmaier, A. Dinkelmann, V. Von Arnim, A. Rau, Corona and dielectric barrier discharge plasma treatment of textiles for technical applications, in: Plasma Technologies for Textiles, Elsevier, 2007, pp. 129–157.
[28] T. Tantiplapol, Y. Singsawat, N. Narongsil, S. Damrongsakkul, N. Saito, I. Prasertsung, Influences of solution plasma conditions on degradation rate and properties of chitosan, Innovat. Food Sci. Emerg. Technol. 32 (2015) 116–120, https://doi.org/10.1016/j.ifset.2015.09.014.
[29] F. Ma, et al., Effect of solution plasma process with hydrogen peroxide on the degradation of water-soluble polysaccharide from Auricularia auricula. II: solution conformation and antioxidant activities in vitro, Carbohydr. Polym. 198 (January) (2018) 575–580, https://doi.org/10.1016/j.carbpol.2018.06.113.
[30] Y. Deng, R. Zhao, Advanced oxidation processes (AOPs) in wastewater treatment, Current Pollution Reports 1 (3) (2015) 167–176, https://doi.org/10.1007/s40726-015-0015-z.
[31] Barreteau H., Delattre C., Michaud P., Production of oligosaccharides as promising new food additive generation, Food Technol. Biotechnol. 44 (3) (Nov. 2005), 323–333.
[32] R. Nastase, J.-M. Tatibouët, E. Fourré, Depolymerization of inulin in the highly reactive gas phase of a non thermal plasma at atmospheric pressure, Plasma Process. Polym. 15 (10) (Oct. 2018) 1800067, https://doi.org/10.1002/ppap.201800067.
[33] R. Nastase, E. Fourré, M. Fanuel, X. Falourd, I. Capron, Non thermal plasma in liquid media: effect on inulin depolymerization and functionalization, Carbohydr. Polym. 231 (December 2019) (Mar. 2020) 115704, https://doi.org/10.1016/j.carbpol.2019.115704.
[34] P. Thana, et al., A compact pulse-modulation cold air plasma jet for the inactivation of chronic wound bacteria: development and characterization, Heliyon 5 (9) (Sep. 2019) e02455, https://doi.org/10.1016/j.heliyon.2019.e02455.
[35] R. Thirumdas, et al., Plasma activated water (PAW): chemistry, physico-chemical properties, applications in food and agriculture, Trends Food Sci. Technol. 77 (May) (2018) 21–31, https://doi.org/10.1016/j.tifs.2018.05.007.
[36] N.N.K. Kaushik, et al., Biological and medical applications of plasma-activated media, water and solutions, Biol. Chem. 400 (1) (Dec. 2018) 39–62, https://doi.org/10.1515/hsz-2018-0226.
[37] B.R. Locke, P. Lukes, J. Brisset, Elementary chemical and physical phenomena in electrical discharge plasma in gas–liquid environments and in liquids, in: Plasma Chemistry and Catalysis in Gases and Liquids, Wiley, 2012, pp. 185–241.
[38] S.W. Liu, Y. Liu, Y.J. Ren, F.C. Lin, Y. Liu, Characteristic analysis of plasma channel and shock wave in electrohydraulic pulsed discharge, Phys. Plasmas 26 (9) (Sep. 2019) 093509, https://doi.org/10.1063/1.5092362.
[39] D.M. Devia, L. V Rodriguez-Restrepo, E. Restrepo-Parra, Methods employed in optical emission spectroscopy analysis: a review, Ing. y Cienc. 11 (21) (Feb. 2015) 239–267, https://doi.org/10.17230/ingciencia.11.21.12.
[40] Z. Ahmad, G.B. Cross, M. Vernon, D. Gebregiorgis, D. Deocampo, A. Kozhanov, Influence of plasma-activated nitrogen species on PA-MOCVD of InN, Appl. Phys. Lett. 115 (22) (Nov. 2019) 223101, https://doi.org/10.1063/1.5126625.
[41] P. Attri, E.H. Choi, Influence of reactive oxygen species on the enzyme stability and activity in the presence of ionic liquids, PLoS One 8 (9) (Sep. 2013) e75096, https://doi.org/10.1371/journal.pone.0075096.
[42] P.J. Bruggeman, et al., Plasma-liquid interactions: a review and roadmap, Plasma Sources Sci. Technol. 25 (5) (2016), https://doi.org/10.1088/0963-0252/25/5/053002.
[43] J.S. Clements, M. Sato, R.H. Davis, Preliminary investigation of prebreakdown phenomena and chemical reactions using a pulsed high-voltage discharge in water, IEEE Trans. Ind. Appl. IA-23 (2) (1987) 224–235, https://doi.org/10.1109/TIA.1987.4504897.
[44] B. Sun, M. Sato, J.S. Clements, Optical study of active species produced by a pulsed streamer corona discharge in water, J. Electrost. 39 (3) (1997) 189–202, https://doi.org/10.1016/S0304-3886(97)00002-8.
[45] J. Julák, A. Hujacová, V. Scholtz, J. Khun, K. Holada, Contribution to the chemistry of plasma-activated water, Plasma Phys. Rep. 44 (1) (2018) 125–136, https://doi.org/10.1134/S1063780X18010075.
[46] S. Theepharaksapan, Y. Lerkmahalikhit, P. Suwannapech, P. Boonnong, M. Limawatchanakarn, K. Matra, Impact of multi-air plasma jets on nitrogen concentration variance in effluent of membrane bioreactor pilot-plant, Eng. Appl. Sci. Res. 48 (6) (2021) 732–739, https://doi.org/10.14456/easr.2021.75.
[47] T. Karunakaran, Y.S. Goh, R. Santhanam, V. Murugaiyah, M.H. Abu Bakar, S. Ramanathan, RP-HPLC-DAD analysis of mitragynine content in Mitragyna speciosa korth. (Ketum) leaf extracts prepared using ultrasound assisted extraction technique and their cytotoxicity, Separations 9 (11) (Nov. 2022) 345, https://doi.org/10.3390/separations9110345.
[48] V.M. Atrazhev, V.S. Vorob'ev, I.V. Timoshkin, M.J. Given, S.J. MacGregor, Mechanisms of impulse breakdown in liquid: the role of joule heating and formation of gas cavities, IEEE Trans. Plasma Sci. 38 (10 PART 1) (Oct. 2010) 2644–2651, https://doi.org/10.1109/TPS.2010.2046337.
[49] A. Sun, C. Huo, J. Zhuang, Formation mechanism of streamer discharges in liquids: a review, High Volt. 1 (2) (2016) 74–80, https://doi.org/10.1049/hve.2016.0016.
[50] R.P. Joshi, S.M. Thagard, Streamer-like electrical discharges in water: Part II. Environmental applications, Plasma Chem. Plasma Process. 33 (1) (Feb. 2013) 17–49, https://doi.org/10.1007/s11090-013-9436-x.
[51] R.P. Joshi, S.M. Thagard, Streamer-like electrical discharges in water: Part I. Fundamental mechanisms, Plasma Chem. Plasma Process. 33 (1) (Feb. 2013) 1–15, https://doi.org/10.1007/s11090-012-9425-5.
[52] F.P. Guengerich, Mechanisms of cytochrome P450 substrate oxidation: MiniReview, J. Biochem. Mol. Toxicol. 21 (4) (Aug. 2007) 163–168, https://doi.org/10.1002/jbt.20174.
[53] S. Ramanathan, S. Parthasarathy, V. Murugaiyah, E. Magosso, S. Tan, S. Mansor, Understanding the physicochemical properties of mitragynine, a principal alkaloid of Mitragyna speciosa, for preclinical evaluation, Molecules 20 (3) (Mar. 2015) 4915–4927, https://doi.org/10.3390/molecules20034915.
[54] K. Matra, K. Narinram, S. Ploysap, P. Prakongsil, J. Promping, Microbial reduction of bitter melon (momordica charantia L.) and chan khao (tarenna hoaensis pitard) herb powder by dielectric barrier discharge plasma for food sanitary, Eng. J. 25 (10) (2021) 87–94, https://doi.org/10.4186/ej.2021.25.10.87.
[55] H.J. Kim, H.I. Yong, S. Park, W. Choe, C. Jo, Effects of dielectric barrier discharge plasma on pathogen inactivation and the physicochemical and sensory characteristics of pork loin, Curr. Appl. Phys. 13 (7) (2013) 1420–1425, https://doi.org/10.1016/j.cap.2013.04.021.
[56] J.S. Kim, E.J. Lee, E.H. Choi, Y.J. Kim, Inactivation of Staphylococcus aureus on the beef jerky by radio-frequency atmospheric pressure plasma discharge treatment, Innovat. Food Sci. Emerg. Technol. 22 (2014) 124–130, https://doi.org/10.1016/j.ifset.2013.12.012.

[57] K. Matra, Electrical treatment methods for sunflower seed germination enrichment, in: 2016 Management and Innovation Technology International Conference, MITiCON 2016, Oct. 2017, pp. MIT22–MIT25, https://doi.org/10.1109/MITICON.2016.8025254.
[58] H. Xu, et al., Oxygen harvesting from carbon dioxide: simultaneous epoxidation and CO formation, Chem. Sci. 12 (40) (2021) 13373–13378, https://doi.org/10.1039/D1SC04209B.
[59] J. Xue, F. Ma, J. Elm, J. Chen, H.-B. Xie, Atmospheric oxidation mechanism and kinetics of indole initiated by •OH and •Cl: a computational study, Atmos. Chem. Phys. 22 (17) (Sep. 2022) 11543–11555, https://doi.org/10.5194/acp-22-11543-2022.
[60] F. A, Carey, Robert M. Giuliano, Chapter 16: ethers, epoxides and sulfides, in: Organic Chemistry, ninth ed., McGraw-Hill, New York, NY, 2014.
[61] N.C. Eddingsaas, D.G. VanderVelde, P.O. Wennberg, Kinetics and products of the acid-catalyzed ring-opening of atmospherically relevant butyl epoxy alcohols, J. Phys. Chem. A 114 (31) (Aug. 2010) 8106–8113, https://doi.org/10.1021/jp103907c.
[62] D.J. Ward, D.J. Saccomando, G. Walker, S.M. Mansell, Sustainable routes to alkenes: applications of homogeneous catalysis to the dehydration of alcohols to alkenes, Catal. Sci. Technol. 13 (9) (2023) 2638–2647, https://doi.org/10.1039/D2CY01690G.
[63] C. Bockisch, E.D. Lorance, H.E. Hartnett, E.L. Shock, I.R. Gould, Kinetics and mechanisms of dehydration of secondary alcohols under hydrothermal conditions, ACS Earth Space Chem. 2 (8) (Aug. 2018) 821–832, https://doi.org/10.1021/acsearthspacechem.8b00030.